Tropical Climate Regimes and Global Climate Sensitivity in a Simple Setting

JOSEPH BARSUGLI, SANG-IK SHIN, AND PRASHANT D. SARDESHMUKH

NOAA–CIRES Climate Diagnostics Center, Boulder, Colorado

(Manuscript received 13 January 2004, in final form 6 July 2004)

ABSTRACT

Multiple tropical climate regimes are found in an atmospheric general circulation model (AGCM) coupled to a global slab ocean when the model is forced by different values of globally uniform insolation. Even in this simple setting, convection organizes into an intertropical convergence zone (ITCZ) solely due to the effect of planetary rotation, as was found in Kirtman and Schneider, for a single value of insolation. Here the response to a range of insolation values is explored, and surprisingly, multiple climate regimes characterized by radically different ITCZ structures are found. In order from the coldest to warmest climates, these are a symmetric double ITCZ, a near-symmetric equatorial ITCZ, a transient asymmetric ITCZ, and a stable, strongly asymmetric ITCZ.

The model exhibits hysteresis in the transition from the near-symmetric to the strongly asymmetric ITCZ regimes when insolation is increased and then decreased. The initial transition away from symmetry can occur in the absence of air–sea coupling; however, the coupling is essential for the establishment and maintenance of the strongly asymmetric ITCZ. Wind–evaporation–SST feedback as well as the longwave radiative effects of clouds and water vapor on SSTs appear to be important in maintaining the asymmetric regime. The existence of multiple regimes in a single AGCM, and the dependence of these regimes on SST feedbacks, may have a bearing on the ITCZ simulation errors of current coupled climate models.

The sensitivity of the global mean surface temperature generally decreases with increasing insolation, a consequence primarily of increasingly negative shortwave cloud forcing. Climate sensitivity measured across a regime transition can be much larger than the sensitivity within a single regime.

1. Introduction

Most current climate models have trouble simulating tropical rainfall. In particular the structure of the intertropical convergence zone (ITCZ) in the Pacific basin varies considerably from model to model. Even in the zonal mean, the rainfall fields show large structural uncertainties with some models exhibiting a distinct "double ITCZ" (Covey et al. 2003). Many of these models also have 1–2-K biases in tropical sea surface temperature (SST). Does the structure of tropical rainfall depend on the mean surface temperature? If so, improving the mean temperature by improving, say, the cloud parameterization or ocean physics may reduce the rainfall errors. But what if the mean surface temperature depends on the rainfall structure? Then modifying ocean physics may be futile. This is just one example of the vexing chicken-or-egg dilemmas that arise in diagnosing climate model errors in a system with interacting land, ocean, atmosphere, and ice components. Errors in modeling one component such as the ocean, or in one physical process such as atmospheric convection, propagate through all other components and processes in the course of determining the model climate. To understand and assess the importance of specific interactions among model components, it is essential to study the models in simplified settings in which some interactions are either greatly simplified or ignored.

Aquaplanet simulations are one simplified setting in which to study the atmospheric general circulation model (AGCM) component of coupled climate models (e.g., Neale and Hoskins 2000). The traditional aquaplanet experiment involves specifying an idealized SST distribution, often as a zonally symmetric field. One aquaplanet result of relevance to the structure of tropical rainfall comes from Hess et al. (1993), who demonstrated that different convective parameterizations could give rise to different ITCZ structures for the same prescribed SST. On the other hand, they, and numerous other aquaplanet studies, have also shown that SST gradients can organize atmospheric convection. To understand how these two effects couple to one another, one must allow the ocean to interact with the AGCM. The simplest interactive ocean is a "slab mixed layer"—that is, a slab of water that only interacts thermodynamically with the AGCM. We will call this a

Corresponding author address: Dr. Joseph Barsugli, NOAA–CIRES Climate Diagnostics Center, 325 Broadway, R/CDC1, Boulder, CO 80305-3328.
E-mail: joseph.barsugli@noaa.gov

"slab aquaplanet" simulation. Slab aquaplanet simulations are less common than traditional aquaplanet simulations, but have the advantage of establishing their own equilibrium surface temperature: one only needs to specify the insolation. They are therefore arguably more instructive than traditional aquaplanet models for understanding coupled climate model errors.

Kirtman and Schneider (2000, henceforth KS) further idealized the problem. They coupled the Center for Ocean–Land–Atmosphere Studies (COLA) AGCM to a 50-m slab ocean and prescribed constant uniform insolation over the whole planet. In this setting, the only departure in the horizontal from uniform, isotropic spherical symmetry in the model equations is due to the rotation of the planet. (Strictly speaking, model discretization breaks this symmetry. While the triangular spherical harmonic truncation used in KS and in our study is indeed uniform and isotropic, the Gaussian grid used to calculate physical processes is neither.) Their main result was that precipitation is preferentially organized, even in this highly idealized setting, into a single ITCZ on the equator solely due to the effect of planetary rotation. The rest of the planet has a nearly uniform precipitation field, except for regions of subsidence on either side of the equator. SSTs are coldest on the equator, with a linear temperature gradient of approximately 5 K from equator to pole. There is a strong upper-level easterly jet with a weaker low-level westerly jet in the subtropics, consistent with the reversed pole-to-equator temperature gradient throughout the troposphere. Transient eddies play a major role in momentum transport and in maintaining the jet. The energetics of the Hadley cell are thermally direct.

In this paper we extend the work of KS by repeating their slab aquaplanet experiment using the National Center for Atmospheric Research (NCAR) Community Climate Model (CCM), and further investigate the model's behavior over a range of insolation. Our methodology (which differs from KS's in several respects) is described in section 2. The original motivation for this study was simple curiosity: Would the results of KS be reproduced in a different GCM, and would different ITCZ structures appear for different values of the solar forcing? Indeed, we find that many of the basic features of the KS climate are robust over a range of parameters. However, we also find that tropical convection can organize in a surprising number of ways, depending on the strength of the insolation, into distinct climate regimes. For lower values of solar forcing (and hence cooler global-mean temperatures T_m), we find solutions that are symmetric (or nearly symmetric) about the equator—both double ITCZ and single ITCZ solutions. For higher insolation (with $T_m > \sim 25°C$), these solutions become highly asymmetric with strong ascent in the Tropics of one hemisphere and descent in the other. It is remarkable that these climate regimes exist even in the absence of ocean dynamics. The regimes are described in detail in section 3. The transition from the symmetric to the asymmetric ITCZ regimes is investigated more closely in section 4, because we believe this to be the most relevant parameter range for understanding coupled behavior in current climate models.

Our demonstration of the existence of meridionally asymmetric solutions of the tropical climate, even under symmetric forcing, also has a bearing on the question of why the observed ITCZ lies primarily in the Northern Hemisphere. We summarize here a few explanations that have been put forward in the literature. For a more detailed summary of the literature on ITCZ theory, see KS. Waliser and Somerville (1994), building on earlier theoretical work, argued for a purely dynamical preference for an off-equatorial ITCZ on the grounds that surface wind convergence under a deep atmospheric heat source is maximized for a source located between 4° and 12° latitude. Raymond (2000) considered the radiative effects of both clouds and water vapor in absorbing upwelling longwave radiation, which differentially heat the atmosphere even in the presence of constant SST. Including these effects in his idealized atmospheric model generated an unstable mode leading to a strongly asymmetric ITCZ. Raymond noted that the water-vapor feedback alone was not strong enough to destabilize his system.

The strong connection between SST and the ITCZ has led many to suspect that feedbacks involving SST changes are essential for asymmetric ITCZ solutions to exist. Xie and Philander (1994, henceforth XP) proposed a symmetry-breaking mechanism involving wind–evaporation–SST (WES) feedback. In WES feedback, surface winds forced by convection alter the evaporation (and we note, the sensible heat fluxes as well) depending on the magnitude of the total wind speed. In their simple model this produces more upward surface heat flux equatorward of the convection, cooling the mixed layer. Relatively weak winds at the latitude of the ITCZ help maintain a warm SST anomaly there. They note that WES feedback relies on the existence of mean oceanic cooling on the equator due to mean upwelling. Without it, weak equatorial winds lead to an equatorial SST maximum, and convection moves to the equator. WES feedback should be differentiated from the purely atmospheric wind–evaporation feedback in which the SST does not change; the latter is thought to have a much weaker effect on ITCZ position (XP).

In addition to WES, SST feedbacks involving altered oceanic upwelling and stratus clouds have also been proposed to break the meridional symmetry. Li (1997) assessed the relative strength of these three SST feedbacks in a unified modeling framework. Using a 1½-layer linear reduced-gravity ocean model with a simple mixed layer coupled to both a linear atmosphere model and to the Geophysical Fluid Dynamics Laboratory (GFDL) AGCM, Li found all three mechanisms to be of roughly equal importance in maintaining the asym-

metry about the equator. In our study, we consider, in addition to stratus clouds, the radiative impact of all cloud types and of water vapor on SST. However, we ignore mechanisms involving upwelling because the slab aquaplanet has no ocean dynamics.

Section 5 summarizes the global mean climate sensitivity of our slab aquaplanet to changes of insolation. An important consequence of the existence of tropical climate regimes in our model is that the climate sensitivity—defined, for example, as the change in global mean surface temperature T_m for a given change in top-of-the-atmosphere insolation—depends on the regime one is in, and on whether one is measuring climate change across a regime transition. Therefore, the existence of regimes may also have implications for determining the climate sensitivity of realistic coupled climate simulations.

2. Method

a. Slab aquaplanet model with uniform insolation

We used version 3.10 of the NCAR CCM with CCM3.6.6 physics (model release ccm3.10.11.brnchT.366physics.7) at T42 18-level resolution. All parameters were set to default values except those mentioned below. Thankfully it was only necessary to modify a single subroutine (zenith.F) to provide the model with uniform insolation. In this subroutine, the solar zenith angle was set to zero and the orbital eccentricity to 1.0 to eliminate the diurnal and seasonal cycles. The prescribed ozone mixing ratio was set at each level to a typical "tropical" profile. The profile was arrived at by taking an average from latitude 30°N–30°S of the annual mean mixing ratio at each hybrid model level from the monthly mean climatology dataset (noaao3.1990.21999.nc) released with the model.

The lower boundary is a global slab ocean. Therefore, the mean orography and subgrid orography were set to zero. Surface temperatures were calculated by assuming a 50-m slab of water everywhere, interacting at every time step with the atmosphere only through radiative heat fluxes and turbulent heat and moisture fluxes. Since we only investigated temperatures above the freezing point of water, no ice model was needed. We also bypassed the land surface model code. We wish to emphasize that apart from these drastic simplifications of the lower boundary conditions, our simulations retain the full physics of the AGCM.

Initial fields for all runs with fixed insolation, including both mixed-layer and prescribed SST runs (see below), were derived from a single initial condition file for January from a realistic climatological SST run with the unadulterated model. All fields were replaced with their "tropical" average in the latitude band 30°N–30°S at each hybrid model level. Gaussian random noise of amplitude about equal to 1% in wind and temperature was added at each grid point.

Our methodology has one notable difference from that of KS. They retained an identical diurnal cycle at each grid point, with the sun directly overhead at noon (B. Kirtman 2004, personal communication), whereas our insolation is truly constant in time.

Their value of the solar constant, 990 W m^{-2}, corresponds to an average insolation of 315 W m^{-2}. The ozone profiles may also differ.

b. Range of insolation

In the slab aquaplanet runs we vary only one parameter, the top-of-the-atmosphere insolation, S. Based on trial and error we settled on a range of 260–340 W m^{-2}, producing global mean temperatures ranging from 10°–35°C (Fig. 1). We performed 20-yr simulations with fixed insolation for S = 260, 280, 290, 300, 310, 320, and 340 W m^{-2} (denoted as S260, S280, etc. in the following). The initial adjustment period of each run was ignored when computing the climatological averages shown in this paper; only the last 10 yr of each run were used.

For S300 and higher the individual hemispheric mean SSTs differ (Fig. 1), indicating a meridionally asymmetric climate regime. To investigate the transition from the symmetric to the asymmetric ITCZ regimes in greater detail, we made two additional runs with S increasing from 290 W m^{-2} at the rate of 0.25 W m^{-2} yr^{-1} to 310 W m^{-2} (denoted S^+) and then decreasing at the same rate from that value down to 285 W m^{-2} yr^{-1} (denoted S^-). We went beyond 290–285 W m^{-2} in this downward sweep because the system had not yet made the transition back to the symmetric ITCZ at 290 W m^{-2}. The initial condition for the S^+ run was taken from the end of the S290 run. A coarser parameter sweep at 1 W m^{-2} yr^{-1} over the range 260–340 W m^{-2} was also performed, but is not extensively discussed here because of the large time lag between the climate response of this run and the fixed-S runs. Three 10-yr runs with fixed, globally uniform SST of 10°, 20°, 25°, and 30°C were also made. Insolation was set at 260 W m^{-2} in the first case and 320 W m^{-2} in the other three cases; the exact value should be of small importance in a fixed-SST aquaplanet setting.

One feature to note in Fig. 1 is that we had to specify much lower values of insolation S than would be consistent with simple energy balance considerations of Earth's present climate. Our warmest case, S340, with insolation near the earth's global average of 342 W m^{-2}, yielded a global mean surface temperature (T_m) of 38°C, which is much larger than the observed T_m of 14.5°C. One explanation for this discrepancy is that the planetary albedo in our runs, which increases monotonically from 0.1 in S260 to 0.21 in S340, is less than that for the earth (~0.3). This is at least in part due to the low surface albedo of an all-ocean planet. The lack of ocean heat transport, especially upwelling, may also play a role in the relative warmth of our aquaplanet. To compare our simulations with KS, whose global

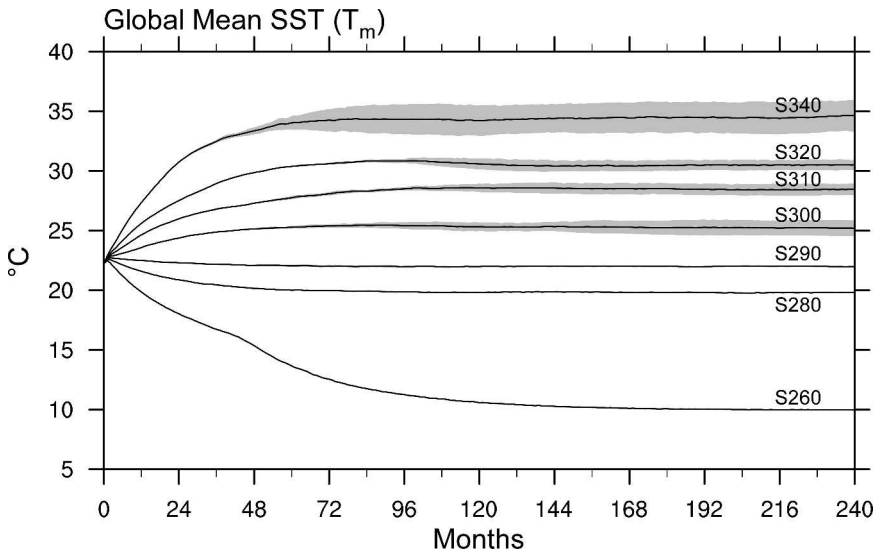

FIG. 1. Global mean SST (black lines) as a function of time for fixed insolation runs S260–S340. Warm (rising) and cold (sinking) hemisphere mean SSTs are indicated by the edges of the gray band.

mean insolation is approximately 315 W m^{-2}, we note that their T_m (26°C) is comparable to the value obtained in our S300 run (25.5°C).

3. Climate regimes

We begin with a descriptive tour of the climate regimes found in the fixed insolation runs. The zonal mean climatologies of SST and precipitation are shown in Fig. 2, and cross sections of the mean meridional mass transport streamfunction, zonal wind, potential temperature, and temperature anomaly (from the mean on each pressure level) in Fig. 3. The runs are divided into three regimes based on the structure of the ITCZ, defined by the tropical peak(s) in the time-mean, zonal-mean precipitation. Two results of KS are reproduced in all cases: precipitation organizes preferentially in the Tropics and tropical SSTs are the coldest on the planet. However, as the specified insolation is changed, the structure of the ITCZ spans a large range of possibilities compared to the single equatorial ITCZ obtained by KS.

The presence of atmosphere-only and coupled ocean–atmosphere transients complicates the identification of climate regimes. Transient noise blurs the transitions between regimes, allowing for a region in parameter space where two regimes can coexist. Transitions between equally possible mirror-image solutions in the asymmetric regimes can also be induced by noise. In our 20-yr runs these transitions seems to occur only for $S < 300$ W m^{-2}. Whether the strongly asymmetric solutions are nonergodic (i.e., whether they are stuck in one of the two possible mirror-image solutions forever) is not a question that can be answered with 20-yr integrations.

a. Symmetric double ITCZ (S260)

In the cool climate of S260 the time-mean precipitation is preferentially located in two bands at latitudes 10°N and 10°S (Fig. 2b). Precipitation is suppressed on

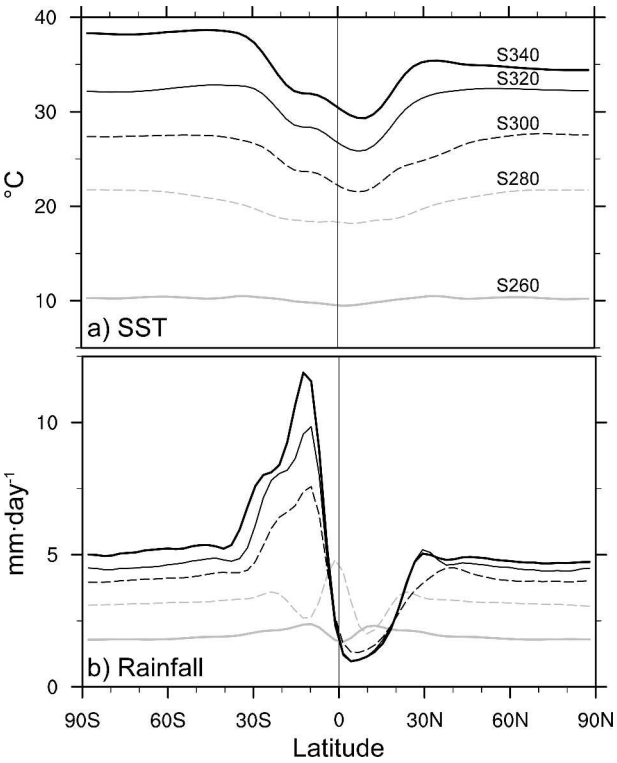

FIG. 2. Zonal mean climatology of (a) SST and (b) precipitation for S260, S280, S300, S320, and S340.

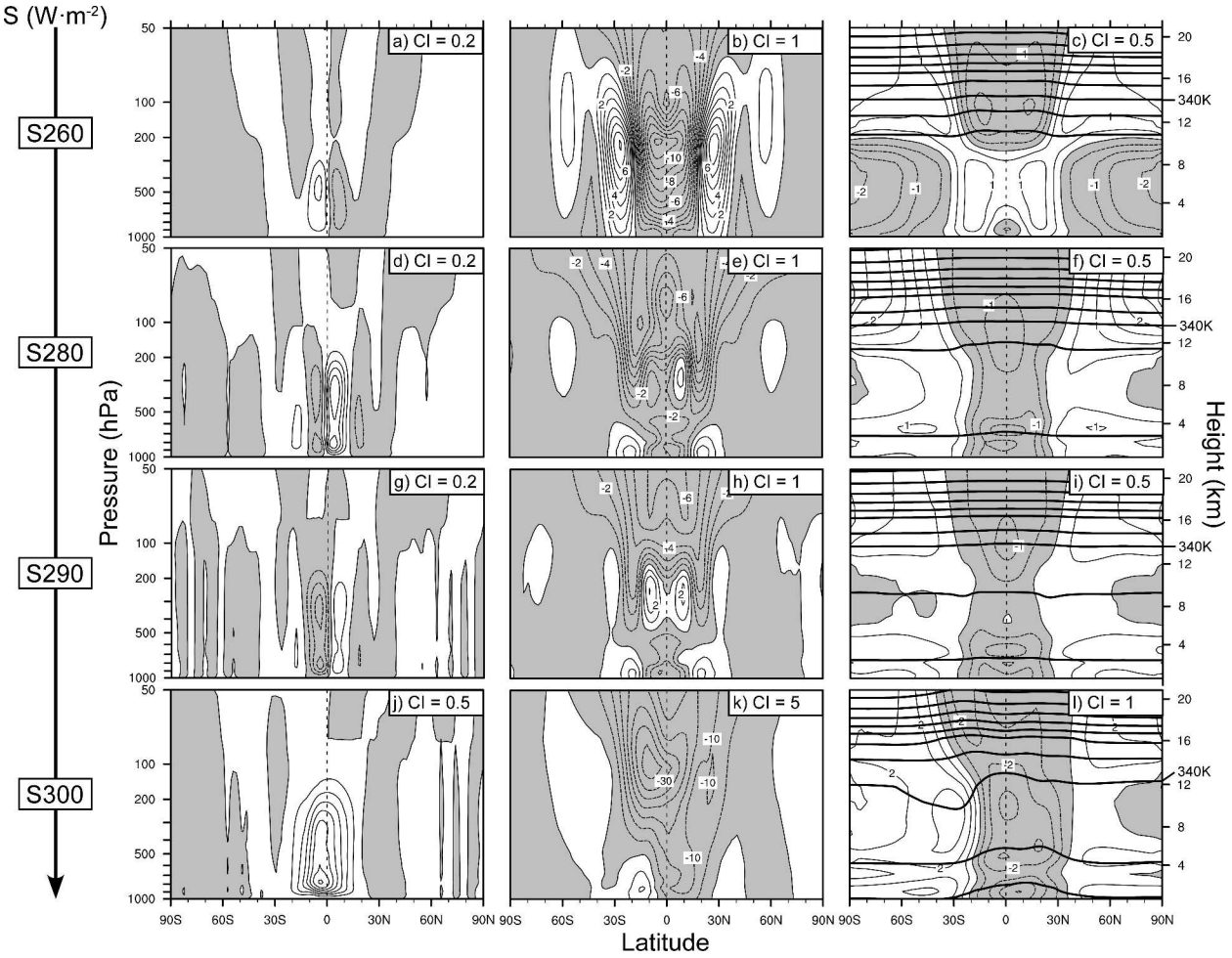

FIG. 3. Climatological values for S260, S280, S290, and S300 of meridional streamfunction (first column), zonal mean zonal wind (second column), and temperature (third column). Both potential temperature (thick contours) and temperature anomaly from the global mean at each level (thin contours, negative values shaded) are shown. Note that contour intevals for S300 differ from the other cases.

the equator by descending motion, as seen in the meridional streamfunction (Fig. 3). Convective precipitation dominates everywhere on the planet, but it is generally weak and shows no special organization outside the deep Tropics. The SST is near 10°C globally, with the equator 0.5 K cooler than the high latitudes. In contrast to the surface, the free tropospheric temperature decreases substantially from its subtropical maximum to the pole with maximum temperature difference of about 3 K in the midtroposphere (400–600 hPa). This gradient is associated with weak westerly upper-level jets at 30°N and 30°S.

S260 is a very cloudy climate regime (Fig. 10b). Midlevel (400–700 hPa) clouds dominate the entire planet, and total cloud fraction is greater than 0.9 everywhere outside the deep Tropics, but the midlevel clouds are radiatively very thin. High clouds are prevalent only in the convective core region and low clouds in the subsidence regions.

Inspection of individual monthly mean fields (Fig. 4a) reveals that the tropical convection is further organized into a single feature extending less than 30° in longitude. A region of descent extends 90° in longitude to the east of the convective core along the equator. Precipitation in the ascending core reaches over 8 mm day^{-1}, compared to the background convective precipitation rate on the rest of the planet of about 1.8 mm day^{-1}. This convective feature maintains its identity throughout the run, propagating steadily westward and circling the planet in 82 months. The convective feature is coupled to a warm SST anomaly in the ascending region and a cold anomaly in the descending region, with a zonal difference in SST of about 4 K. A run performed with fixed SST of 10°C (not shown) has a double ITCZ, but no localized convective feature, so this feature is an intrinsically coupled phenomenon. Variation of latent heat flux along the equator in S260 is by far the dominant cause of the westward propaga-

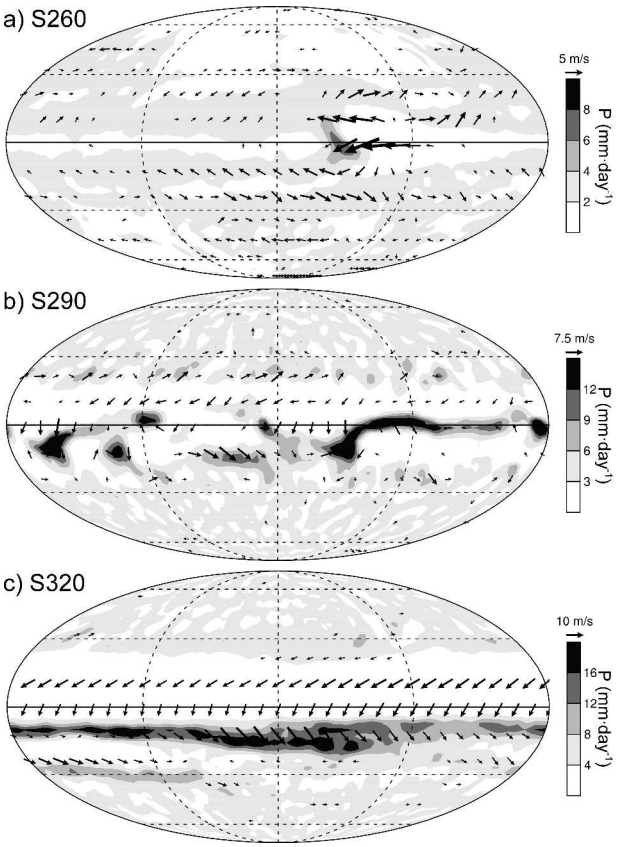

FIG. 4. Selected monthly mean "snapshots" of precipitation and surface wind fields for (a)S260, (b)S290, and (c)S320 cases chosen for a month near the end of each run.

tion of the SST anomaly. The wind field in Fig. 4a is consistent with WES feedback operating in the zonal direction.

b. Near-symmetric single ITCZ (S280, S290)

Precipitation in both the S280 and S290 runs peaks at the grid points nearest the equator in the time mean. (Note that there is no grid point precisely on the equator in this model). Two regions of mean subsidence at 10°N and 10°S show reduced precipitation. For S280, the global mean temperature is about 19.8°C with the equator approximately 3 K colder than the Poles. For S290, the mean is 22°C and the difference 3.2 K. The ITCZ structure in this regime is similar to that in KS. The overall structure of the general circulation is also similar, with reversed equator-to-pole temperature gradients at the surface and aloft, and upper-level easterly and surface westerly jets in the subtropics of both hemispheres. There is even a similarity in the zonally elongated features seen in the instantaneous precipitation fields (Fig. 4b). However, there are some differences. The climates of S280 and S290 are colder and have less precipitation than that of KS. The equator-to-pole temperature gradient is weaker in S280 and S290 than in KS, and as a result, the easterly jets are also weaker. The meridional temperature gradient in KS is almost linear from equator to pole, whereas our temperature gradients are concentrated at the edge of the Tropics and are small poleward of 40° latitude. Note that the climate of the S300 run is closest to KS in terms of global mean temperature, but lies in a significantly different climate regime.

This near-symmetric regime is much less cloudy than S260 (Fig. 10b). High clouds associated with deep convection now dominate, except in subsiding regions. The decrease in planetary albedo results in a large jump in global mean temperature from S260 (10°C) to S280 (19.8°C). This effect is enhanced by the increase in high clouds, but it is somewhat counteracted by the increase in low clouds.

The time-mean meridional streamfunction for S280 appears to be asymmetric about the equator. The S290 streamfunction is also asymmetric, but somewhat less so and in the mirror-image sense (Fig. 3). The apparent asymmetry is related to the fact that the climatological Hadley circulation in these two runs is the average of times when convection peaks one grid point north of the equator and times when it peaks one grid point south. As Lindzen and Hou (1988) demonstrated, even a slight displacement of the atmospheric heating off the equator leads to a strongly asymmetric mean meridional circulation. There are many spontaneous transitions between these two mirror-image states in the course of our 20-yr runs. The ease of transition is probably a result of the weak SST gradients (and hence small thermal inertia) associated with these weakly asymmetric states. The time scale of the transitions appears more rapid in S290 than in S280, resulting in slightly better sampling and a more symmetric 10-yr average. The transients (Fig. 4b) themselves have a rich, perhaps chaotic temporal structure with general eastward propagation. Since the CCM3 does not have a grid point precisely on the equator, the tendency for the ITCZ to lay either one grid point north or south of the equator may be an artifact of the model grid.

c. Asymmetric ITCZ (S300–S340)

The solutions for $S = 300$, 310, 320, and 340 W m^{-2} are all strongly asymmetric about the equator in the Tropics, and their dynamics appear to be similar to one another. Differences among the runs are mainly a matter of the strength of the circulation and the hydrologic cycle. Tropical precipitation falls mostly in one hemisphere, which we will refer to as the rising hemisphere, and precipitation is strongly suppressed in the opposite sinking hemisphere. The precipitation peaks at 10° latitude in the rising hemisphere. However, a band of large precipitation values extends to 30°. Note that the symmetry of the boundary conditions allows for two equally likely asymmetric solutions that are mirror images of one another. For the purposes of display the rising hemisphere is mapped to the Southern Hemi-

sphere, requiring us (as it happened) to present the mirror image of S340.

The mean meridional streamfunction fields for S320 and S340 (not shown) are structurally very similar to that shown in Fig. 3 for S300, with only a small increase in transport from S300 to S340. They depict a single Hadley cell in the Tropics. A single upper-level easterly jet lies at the apex of the rising motion. In contrast to the almost negligible increase in Hadley transport, this jet intensifies substantially from -30 m s^{-1} in S300 to -50 m s^{-1} in S340. Therefore, as in KS, eddy momentum fluxes must become progressively more important in the momentum budget of the jet.

Once established in a particular hemisphere, the ITCZ is very stable, persisting for the duration of the run. This stability is remarkable given the existence of active transients. The transients (Fig. 4c) are zonally elongated and appear to be coupled to SST anomalies. For S340 the coupled transients propagate eastward, whereas for all other cases they mainly propagate westward.

4. Transition from the near-symmetric to asymmetric regime (S290 to S300)

We focus on the transition from the symmetric to the strongly asymmetric ITCZ between $S = 290$ and $S = 300$ W m^{-2} for two reasons. First, it occurs in a realistic range of surface temperatures. More importantly, it involves SST feedbacks and therefore has a bearing on understanding structural ITCZ errors in coupled models. The potential role of SSTs is evident from examining the meridional SST gradient between the rising and sinking branches of the Hadley cell. This gradient is extremely weak in the near-symmetric regime (see Fig. 2), while it attains values of 2–3 K in the strongly asymmetric regime, with the precipitation maximum lying directly over a local SST maximum, and the precipitation minimum lying directly over the global SST minimum.

a. *Mechanisms: Radiation–SST and wind–evaporation–SST feedbacks*

We first examine the surface energy budget for evidence of feedback involving SSTs. The surface energy budget may be formulated to isolate contributions from shortwave and longwave cloud forcing, water vapor radiative forcing, and surface turbulent fluxes (see the appendix). These terms are shown for S290 (near-symmetric regime) and S300 (asymmetric regime) in Fig. 5. The meridional difference (Δ) of these forcing terms between the latitudes of maximum and minimum tropical precipitation may be used to assess the impor-

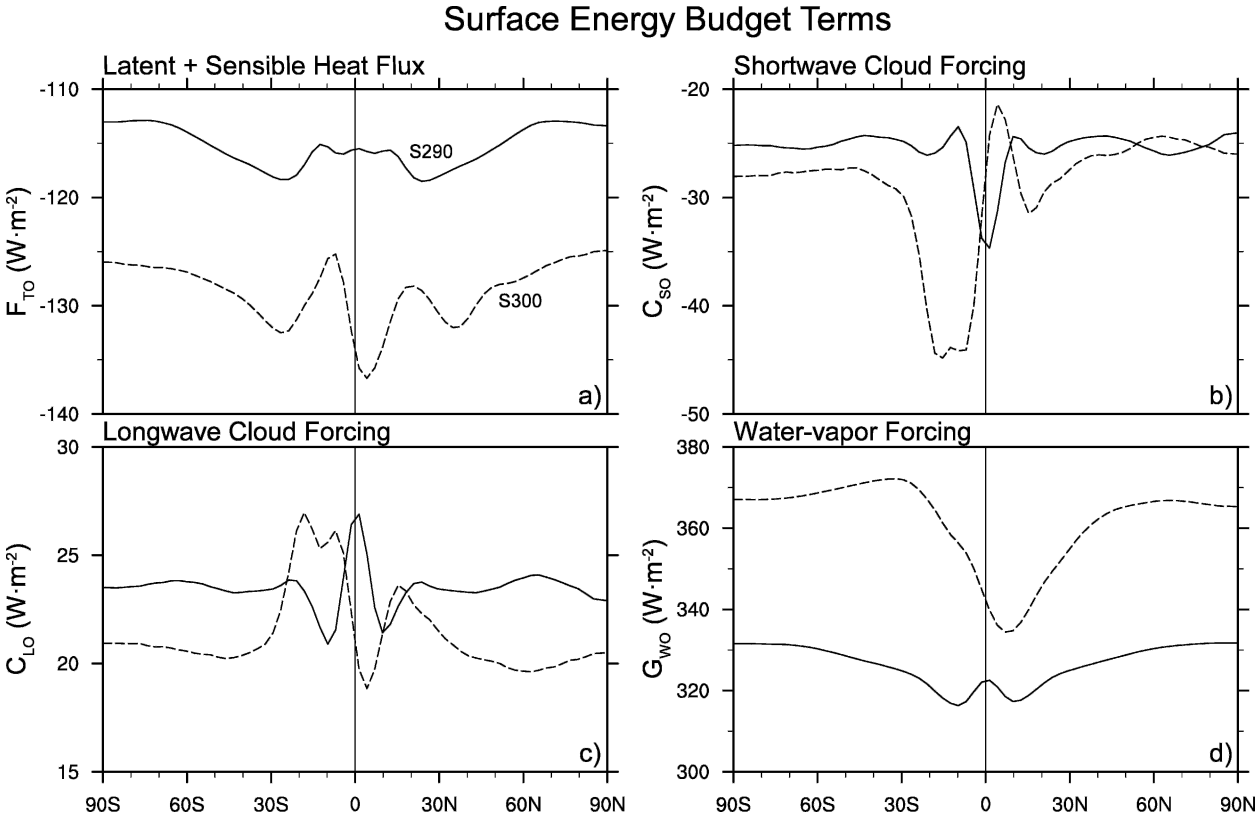

FIG. 5. Zonal mean surface energy budget terms for S290 (near-symmetric regime) and S300 (asymmetric regime): (a) latent plus sensible heat flux, (b) shortwave cloud forcing, (c) longwave cloud forcing, and (d) clear-sky (water vapor) radiative forcing.

TABLE 1. The meridional difference Δ of the terms in the surface energy budget between the latitudes of maximum and minimum precipitation in the fixed-S runs. Positive values indicate a tendency for relative surface warming at the latitude of the ITCZ. Imbalances in the total budget are mainly due to rounding.

	$-\Delta\sigma T^4$	ΔC_{LO}	ΔC_{SO}	ΔG_{WO}	ΔF_{TO}	ΔS_0^{clear}
S290	0	7	−14	7	0	−2
S300	−12	7	−24	21	12	−3

tance of the various feedbacks on ITCZ formation discussed in the introduction; ΔF_{TO} forcing suggests wind–evaporation–SST feedback, ΔC_{SO} and ΔC_{LO} forcing suggests cloud–radiation–SST feedbacks, and ΔG_{WO} forcing suggests clear-sky water-vapor radiation–SST feedback. These differences are tabulated in Table 1 for the S290 and S300 cases. Positive values in Table 1 indicate that term in the energy budget reinforces the ITCZ (with warming under the ITCZ, and cooling in the subsiding region), and negative values indicate a damping of the ITCZ.

The largest term is the negative forcing due to the shortwave cloud forcing differences, and this forcing increases substantially from S290 to S300. The net cloud forcing $\Delta(C_{LO} + C_{SO})$ at the surface is negative in both cases, though the longwave cloud forcing considered alone acts as a positive feedback. It is interesting that the surface turbulent flux forcing increases from near zero in S290 to 12 W m^{-2} in S300. The positive water vapor forcing also increases between these two cases. Therefore, WES and water vapor feedback are likely to play an important role in the transition between these two climate regimes.

It is instructive to examine the energy budget for the whole atmospheric column as well (see the appendix for definitions). In contrast to the surface, the atmospheric column feels a net positive cloud feedback (Fig. 6) onto the ITCZ, with relative heating at the location of the rising branch and relative cooling at the location of the sinking branch(es). The strong positive water vapor feedback also stands out. Shortwave cloud forcing intensifies from S300 to S340, while longwave cloud forcing changes little as S is increased above 300 W m^{-2}. Globally, the net cloud radiative forcing of the atmospheric column decreases as S increases, as does the feedback onto the ITCZ. The additional heat intercepted in the atmospheric column is in balance with dynamical transport. Atmospheric dynamics are critical in closing the feedback loop, and in fact dynamical feedbacks such as those discussed by Waliser and Som-

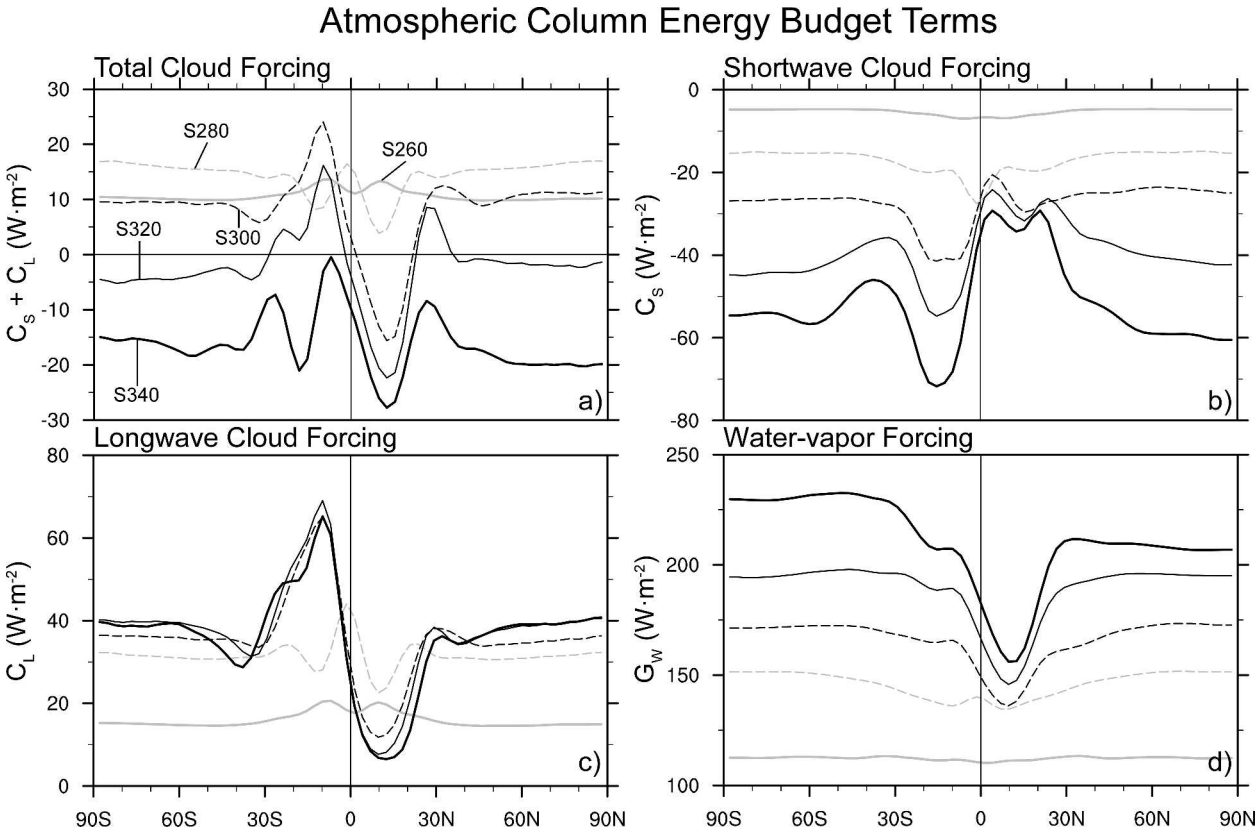

FIG. 6. Zonal mean radiative forcing of the atmospheric column: (a) total cloud radiative forcing, (b) shortwave cloud forcing, (c) longwave cloud forcing, and (d) clear-sky (water vapor) radiative forcing.

erville (1994) are probably critical for the existence of an off-equatorial ITCZ.

b. Hysteresis

To investigate the transition from the symmetric to asymmetric regimes we performed runs with insolation S increasing at the rate of 0.25 W m^{-2} yr^{-1} from 290 to 310 W·m^{-2} (S^+) and then decreasing to 285 W m^{-2} (S^-). Figure 7 shows time–latitude plots of zonal mean temperature, precipitation, surface meridional wind, and total cloud fraction. The transition is evident in all these fields. In addition to the nearly symmetric and strongly asymmetric regimes, there appears to be an intermediate regime where convection peaks 2–3 grid points away from the equator. In this metastable regime convection is able to switch hemispheres spontaneously, unlike in the strongly asymmetric regime. These transitions between the mirror-image solutions are particularly evident in the meridional wind field (Fig. 7c).

When insolation is decreased below 300 W m^{-2}, there is a marked hysteresis in the location of the ITCZ. The system stays in the strongly asymmetric regime until $S \approx 292$ W m^{-2}. This is shown in Fig. 8, in which the latitude of the ITCZ (the latitude of the maximum in 12-month mean precipitation) is plotted for the S^+ and S^- runs. Since the transition away from the near-symmetric regime in the S^+ run occurred just above 290 W m^{-2}, the results from the S290 run are also plotted here to show the ITCZ position in the near-symmetric regime. Note that a 3-yr running median filter has been applied to the ITCZ position in order to remove some outliers in which the maximum in precipitation lies outside the Tropics. These outliers occur in brief periods when the tropical convection is weakly organized or is in transition between hemispheres.

c. The role of air–sea feedback

Is a transition from nearly symmetric to strongly asymmetric ITCZ regimes possible in the absence of interactive SSTs? Figure 9 shows zonal mean precipitation versus time for runs with prescribed constant globally uniform SST of 20°, 25°, and 30°C. These three values of SST correspond roughly those obtained in S280, S300, and S320. At 20°C, the ITCZ is symmetric on the equator as in S280, consistent with the fact that in S280 the SST gradients are very small in the Tropics. At 25°C, the ITCZ prefers an off-equatorial location, but is quite variable. This behavior is comparable to the intermediate regime found in the transient *S* runs. (However, the intermediate regime in the coupled run is somewhat more stable, possibly due to the thermal inertia of the mixed layer). Finally, at 30°C, the system returns to a symmetric ITCZ on the equator—a rather surprising behavior!

From the above we deduce that the transition from the near-symmetric to asymmetric regimes in the slab aquaplanet runs involves two steps. As insolation begins to increase above 290 W m^{-2}, the changing balances in the atmospheric dynamics and physics alone are sufficient to allow the ITCZ to prefer an off-equatorial location. Interaction with SSTs acts to increase the stability of this "intermediate" regime, but does not appear to be essential to its existence. As insolation is increased further, however, the SST feedbacks diagnosed in section 4a above become essential, and they create an extremely stable, strongly asymmetric solution.

5. Climate sensitivity

In this section we discuss some aspects of the sensitivity of the global mean surface temperature, T_m, to

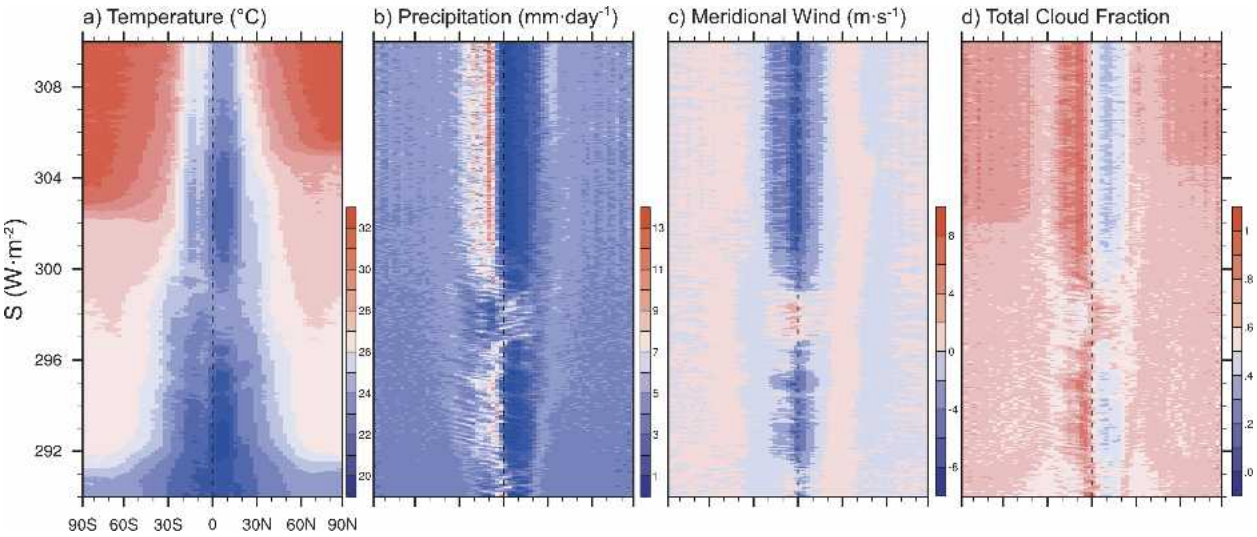

FIG. 7. Time–latitude section for zonal mean (a) SST, (b) precipitation, and (c) near-surface meridional wind, and (d) total cloud fraction for run S^+.

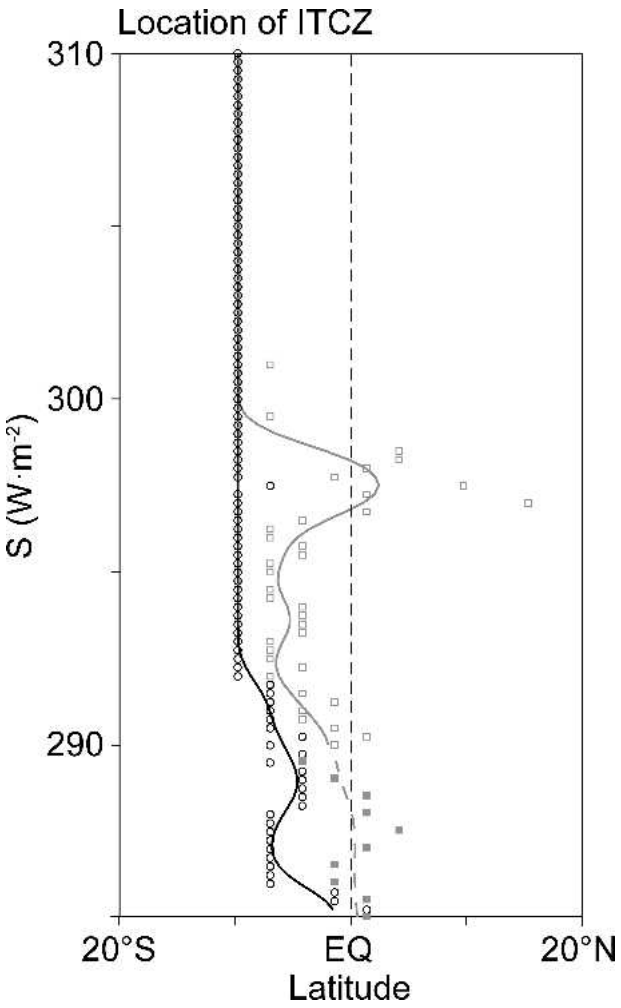

FIG. 8. Latitude of the ITCZ (see text) as a function of insolation S for S^+ (open gray squares) and S^- (black circles) runs. Above $S = 300$ W m^{-2} the ITCZs in the two runs are collocated. The location of the ITCZ during the S290 run (solid gray squares) is shown below the S^+ run to illustrate the near-symmetric regime. Solid and gray dashed lines are smoothed versions of the discrete data.

insolation changes in our simple setting. We also discuss the dependence of some climate feedbacks on the surface temperature. Figure 10a shows T_m obtained in each of the fixed insolation runs. For the most part the global mean temperature sensitivity, dT_m/dS, decreases with increasing insolation. The main exception to this overall trend in climate sensitivity is the "kink" in the graph of T_m at S290 where the transition from symmetric to asymmetric regimes takes place. Because of the regime transition, the climate sensitivity measured from S290 to S300 [0.33 K (W m^{-2})$^{-1}$] is 50% larger than the sensitivity measured between S280 and S290 [0.21 K (W m^{-2})$^{-1}$]. The global-mean precipitation shows a similar kink in sensitivity (not shown).

First we consider the role of cloud radiative forcing in the overall trend in T_m. For reference, Fig. 10b shows the high (above 400 hPa), middle (400–700 hPa), and low cloud (below 700 hPa) fraction as a function of insolation. The cloud radiative forcing (CRF) for runs S260 to S340 are plotted in Fig. 11, this time as a function of the global mean temperature. The longwave cloud forcing (LWCF) levels off and even decreases for large values of T_m, whereas the shortwave cloud forcing (SWCF) becomes monotonically more negative. This is consistent with the fact that cloud changes are dominated by the change in low cloud fraction for S300 and above. In fact, the net CRF changes sign, and because of the negative slope, cloud radiative forcing acts as a negative feedback on the climate in the simulations above S280. Between S280 and S340, the change in net CRF (-30 W m^{-2}) compensates for about half the increase in insolation. Note that over the same range of insolation the change in the other main term in the global energy budget, ΔG_w (90 W m^{-2}) acts as a positive feedback.

It is interesting to compare our results to those of Larson and Hartmann (2003a,b; henceforth LH2003a, LH2003b respectively) whose experiments were designed to consider tropical feedbacks alone. LH2003a found net positive cloud feedback in an idealized simulation of the Tropics using a mesoscale model with no planetary rotation (f=0) and spatially uniform SSTs. Their result is not surprising given that high cloud changes dominate in their model, whereas low cloud changes are more important in our simulations. The companion study, LH2003b, found that the presence of SST gradients and the associated large-scale circulations and cloudiness tends to decrease climate sensitivity. Indeed the appearance of significant SST gradients in the asymmetric regime does have a strong impact on climate sensitivity, though the effects differ from Larson and Hartmann, probably due to the contrasting ways in which the high and low clouds respond in the two models.

The insets in Fig. 11 show the SWCF, LWCF as a function of T_m for the S^+ run. There are two regimes evident in this inset—the intermediate regime discussed in the previous section, and the strongly asymmetric regime—with a rapid transition between the two regimes at about $T_m = 298.5$ K. The fixed-S runs lie nearly on these curves, indicating that the kink in the temperature sensitivity is due to the regime transition. At lower values of insolation, the near-symmetric regime appears to have a strong negative slope in SWCF as indicated by comparing S280 and S290. The striking difference between the near-symmetric and intermediate regimes is also evident in the runs where insolation was increased by 1.0 W m^{-2} yr^{-1} (not shown).

Though less apparent, the clear-sky greenhouse effect, dG_w/dT_m also shows a sharp increase in slope at the regime transition, indicating an increase in the water vapor feedback. As noted in, for example, Held and Soden (2000), middle- and upper-tropospheric water vapor dominates the water vapor feedback. To get some indication of the impact of the regime transition

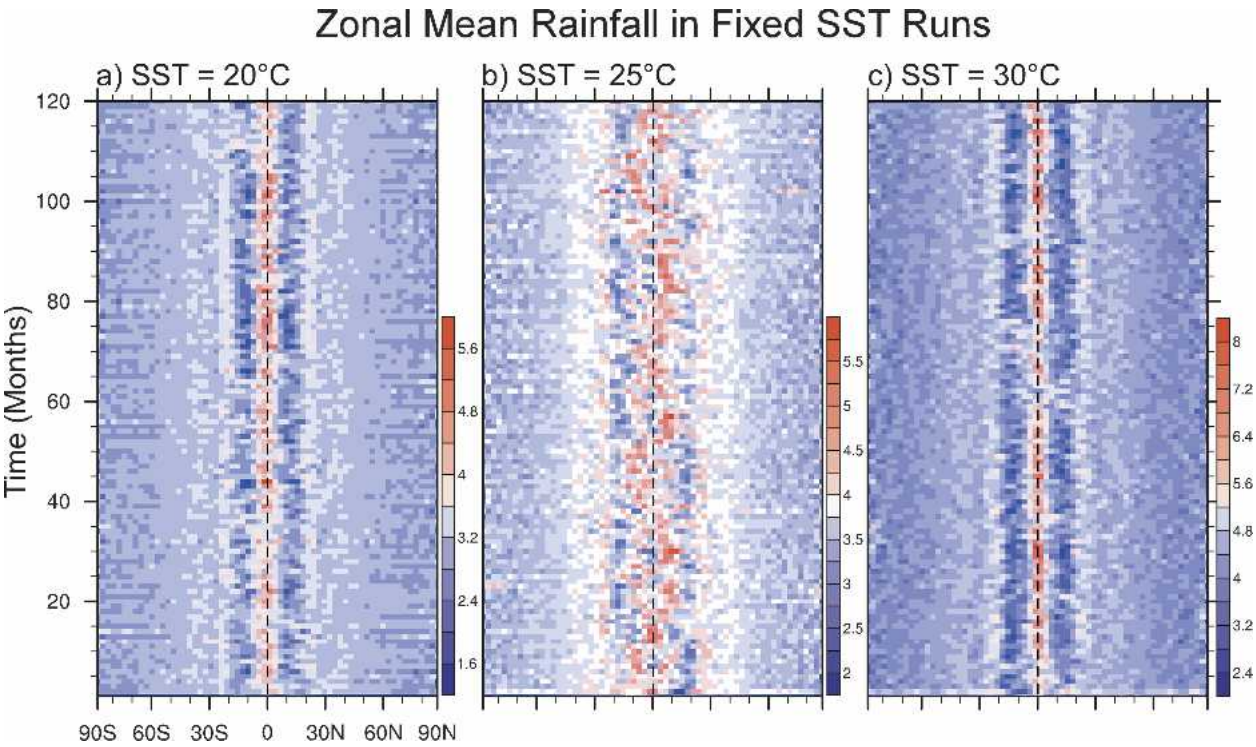

FIG. 9. Time–latitude sections showing the zonal mean of precipitation for fixed-SST runs with SST values of (a) 20°C, (b) 25°C, and (c) 30°C.

on the structure of water vapor we show the vertical profile of relative humidity for S280 and S340 in Fig. 12. Though we have shown the extremes here, they are indicative of the trend for the cases that lie in between. There is a drying of the upper troposphere in regions of strong climatological downward motion, a moistening of the midtroposphere in regions of strong upward motion, and a general upward translation of the humidity profile for the rest of the planet. The impact on G_W (not shown) for the climatological upward and downward regions nearly cancel out, leaving the trends in the rest of the planet to determine the global mean.

Finally, it is instructive to look at the vertical profile of global mean temperature for S260 through S340, shown on a skew T-log$p$ diagram in Fig. 13. The upper-to-midtropospheric lapse rate tends to loosely follow the moist (saturated) adiabatic lapse rate, which decreases with increasing temperature. Early investigations of the lapse-rate effect in radiative–convective models were done by Chýlek and Kiehl (1981) and Lindzen et al. (1982). Both studies found that lapse rate changes decreased the impact of other forcing on surface temperature compared to assuming a fixed lapse rate. LH2003a quantified the negative lapse rate feedback (similar in both convective and nonconvective areas) as –2.4 W m^{-2} K^{-1} for SST = 301 K. This is about half the magnitude and opposite in sign to the feedback from changes in specific humidity. Lindzen et al. (1982) argued that the lapse-rate effect is strong enough to

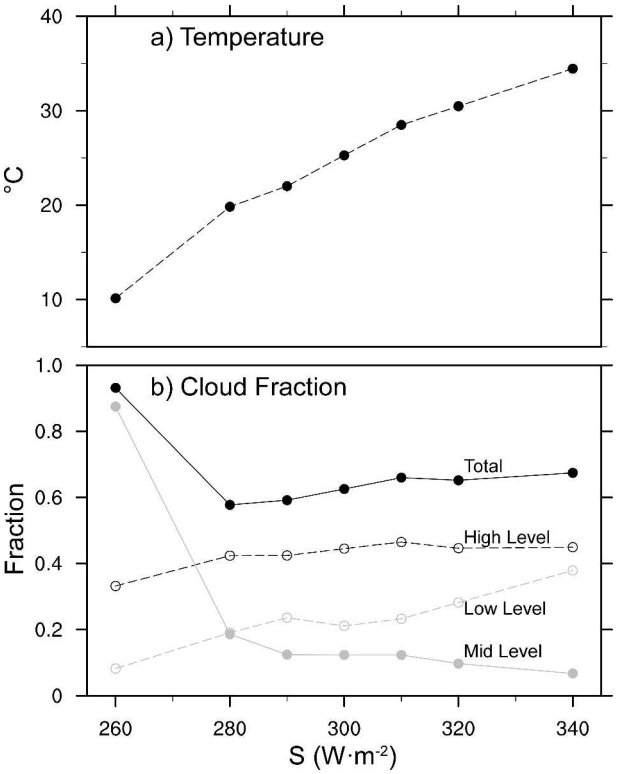

FIG. 10. Global mean values for fixed-S runs as a function of insolation: a) SST and b) cloud fraction.

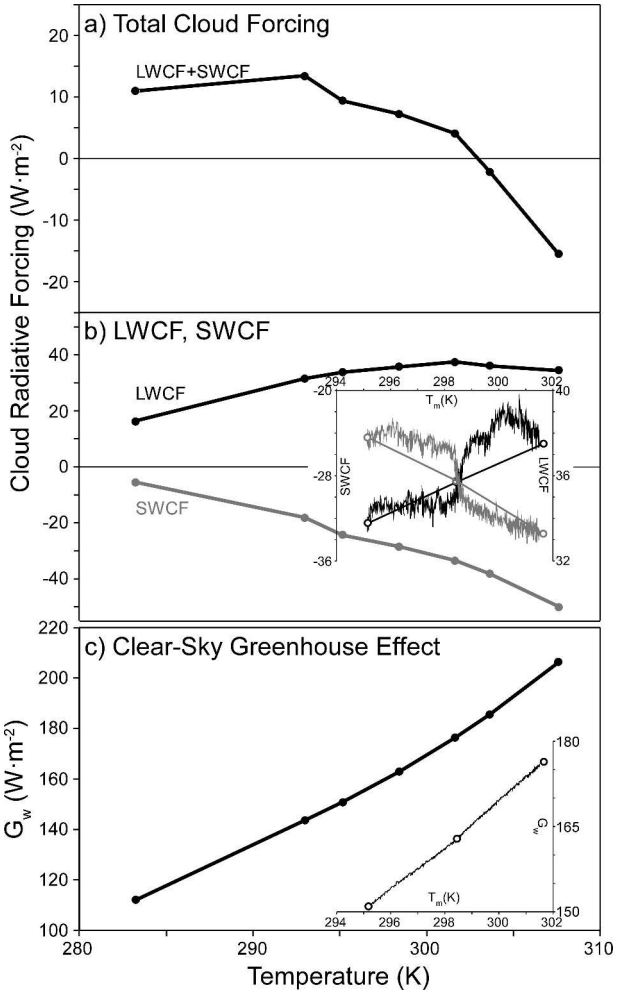

FIG. 11. Global mean radiative forcing terms: (a) total cloud radiative forcing, (b) LWCF, (c) SWCF, and (d) clear-sky greenhouse effect (G_w) for the fixed-S runs. Insets show SWCF, LWCF and G_w for the S^+ run across the transition to the strongly asymmetric regime.

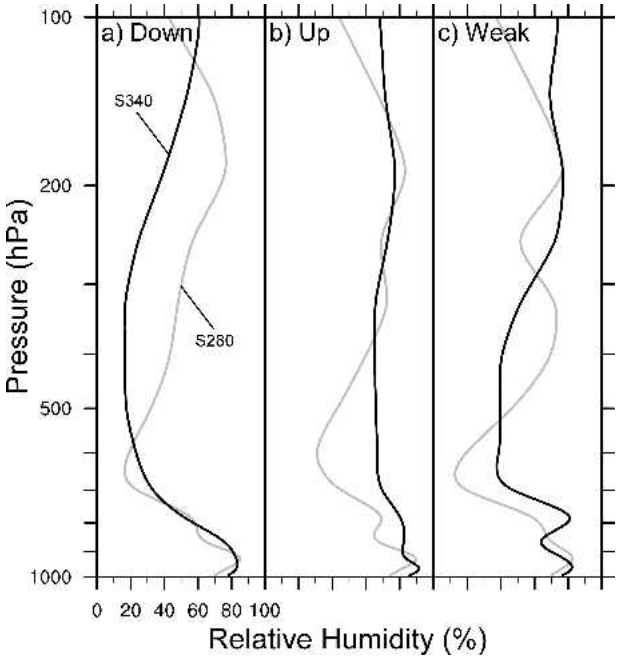

FIG. 12. Vertical profile of relative humidity in S280 and S340 cases for latitudes of (a) downward ($\omega > 0.1$ Pa s^{-1}), (b) mean upward (ω 0.1 Pa s^{-1}), and (c) weak vertical motion.

produce a concave-downward dependence of T_m on insolation, with T_m asymptoting to 315 K for large values of insolation in their model. In contrast, when they assumed a fixed 6.5 K km^{-1} lapse rate, as was used by Manabe and Wetherald (1967) in their much cited paper, Lindzen et al. (1982) found a runaway greenhouse effect. In our simulations, the derivative of clear-sky OLR with respect to global-mean temperature, $d(F_{clear})/dT_m$, decreases monotonically from 2.5 W m^{-2} K^{-1} between S280 and S290 to 1.3 W m^{-2} K^{-1} at higher values of S. Therefore, given the temperature and humidity profiles generated by this model, the clear-sky radiation effect by itself would suggest a concave upward surface temperature dependence. The reason that we have a (slightly) concave downward dependence of temperature on insolation is mainly due to cloud–radiative forcing.

The existence of climate regimes in this model may have implications for determining climate sensitivity in "global-change" simulations. In general, a model estimate of climate sensitivity will depend on the climate regime and on whether or not the model goes through a regime transition in the climate sensitivity experiment. *The hysteresis in the system is also interesting in that the transition may be relatively abrupt, and not easily reversible.* Since the precise value of S at which the transition occurs in a given transient run is determined by "noise," the transition in any single run will be more abrupt than in the ensemble mean of such runs. One is reminded that nature, after all, is making only one run!

6. Conclusions

We have taken an atmospheric general circulation model (NCAR CCM3), coupled to a global slab mixed-layer ocean, and investigated the response of the model to a range of globally uniform insolation. This is an extension of the work of Kirtman and Schneider (2000). The purpose of this experiment was to understand the behavior of a complex climate model in a simplified setting with the hope of shedding some light on the origin of errors of ITCZ structure in coupled climate models. We have clearly shown the existence of tropical climate regimes with greatly varying ITCZ structure in a single AGCM with a single, standard set of parameterizations, and have discussed some of the implications of their existence for climate change simulations.

When we compare the symmetric ITCZ regime (S280

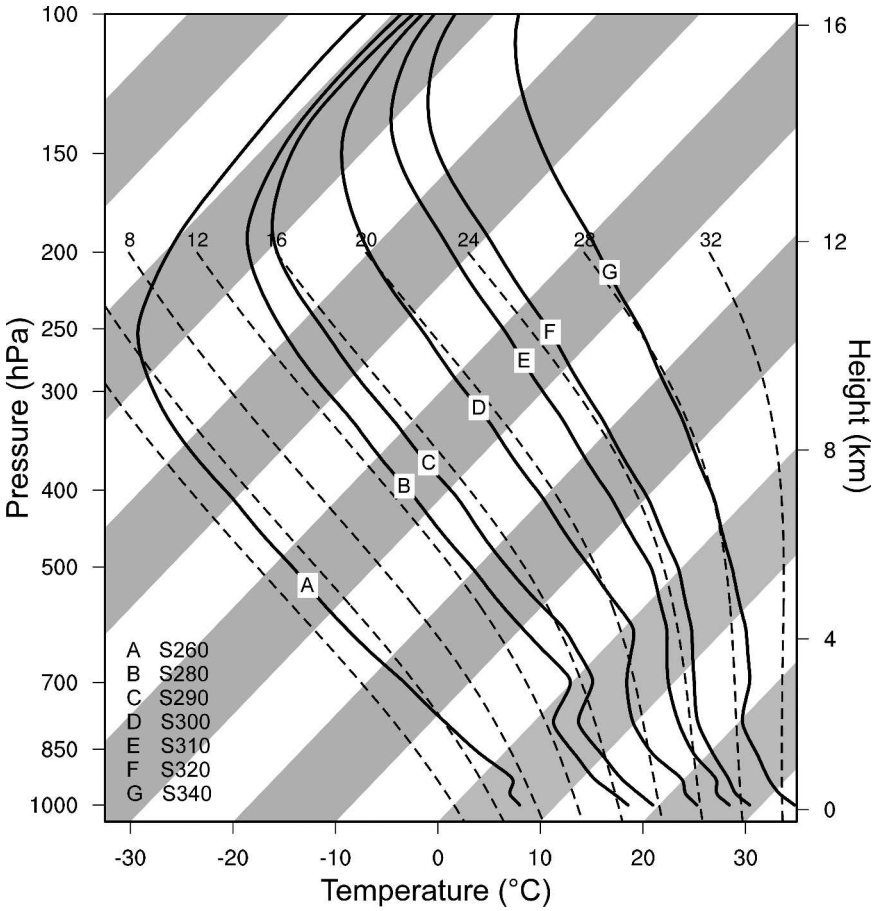

FIG. 13. Global mean vertical profile of temperature for fixed-S runs on skew T–log$p$ coordinates. Selected moist adiabats are also shown.

and S290) with the slab aquaplanet run of KS (using the COLA AGCM), we find the following similarities.

- Convective precipitation, though it occurs globally, is favored near the equator (this is true in all cases).
- The surface temperature (SST) generally increases from equator to pole, though our temperature gradient is concentrated in the subtropics, and theirs is linear from equator to pole.
- Strong upper-level easterly jets and weaker low-level westerly jets are formed in the subtropics.
- Transient eddies, which appear to be driven by unstable vorticity gradients, are an essential part of the momentum budget, and generally transport westerly momentum away from the equator.

When we investigate the behavior of the NCAR CCM under a range of insolation, we find the following.

- There are distinct climate regimes. These regimes are characterized by differences in the location of the ITCZ and are accompanied by major changes in tropical dynamics.
- The CCM, with a fixed set of parameterizations is capable of producing a symmetric double ITCZ, a single ITCZ on the equator, and a single ITCZ off the equator.
- Transitions between these regimes are relatively abrupt, though there is some hysteresis depending on whether the solar constant is increasing or decreasing.
- In weakly asymmetric regimes, "noise" can cause a shift between two equally likely mirror-image solutions.
- The transition from the symmetric to the strongly asymmetric regimes involves two steps: the first transition to a variable off-equatorial ITCZ occurs even in the fixed-SST cases (and therefore likely does not depend upon SST feedbacks), whereas the second transition to the highly asymmetric regime requires SST feedbacks.
- The model climate feedbacks as measured by derivatives of SWCF, LWCF, and H_2O forcing, may be different in the different climate regimes.
- The surface temperature sensitivity of the model generally decreases slightly with increasing insolation as a result of increasingly negative shortwave cloud forcing, mainly due to an increase in low clouds.

The transition from the near-symmetric to the highly asymmetric ITCZ regime is probably the most interesting phenomenon found here with regard to understanding coupled climate model errors. We speculate that such a transition will occur in a number of different GCMs, but will be absent in others, when run in slab aquaplanet mode. We say this because SST feedbacks are essential for this transition. Wind–evaporation–SST (WES) and water vapor feedbacks are already present and of roughly the same realistic magnitude in most GCMs. Cloud feedbacks, however, vary considerably among current models, and may differ substantially from reality. For example, Sun et al. (2003) document that the CCM3 has the wrong sign of net atmospheric feedback in the East Pacific cold tongue region, and that this is the result of errors in both SWCF and LWCF. The location in parameter space of the transition (or even its very existence) in a particular model will depend on the relative strength (and signs) of the WES and radiative feedbacks. Therefore, a model may produce a structural error such as a double ITCZ simply because small errors in these feedbacks put it on the wrong side of a regime transition, and not because of any fundamental problem with the model's physics. For example, both the COLA and NCAR models are capable of producing a symmetric ITCZ on the equator, but in different parameter ranges.

Of course, there are numerous caveats to the application of results obtained in a simplified setting such as ours. We have not explicitly diagnosed the role of atmospheric dynamics and transient disturbances. The climates in our simulations are distinctly different from the present terrestrial climate, primarily due to the lack of equator-to-pole insolation gradient. Because of this, extratropical baroclinic activity is weak and the upper-tropospheric jet structure is unusual. In addition, simulations such as ours in which natural asymmetries such as the distribution of land or the meridional gradient of insolation have been removed may exhibit regimes more easily than more realistic simulations because conditions tend to change all at once over the entire planet . One must also wonder to that extent including ocean dynamics will suppress or enhance the regimes presented here. In the context of more realistic simulations, it is interesting to note that Langen and Alexeev (2004) and C. Li (2003, personal communication) have separately found meridionally asymmetric solutions in slab aqua-planet simulations with the NCAR CCM3 using symmetric insolation based on annual mean values. Apparently sea ice is important in establishing these asymmetric solutions. Specified Northern Hemisphere sea-ice anomalies representative of the last glacial maximum can also cause the ITCZ to shift to the Southern Hemisphere (Chiang and Bitz 2004, submitted to *Climate Dyn.*). In spite of the above caveats, our simulations raise the intriguing possibility that genuine tropical climate regimes may exist within a relatively narrow range of external forcing, with important implications for assessment of global climate sensitivity.

Acknowledgments. We thank David Battisti for suggesting this line of inquiry, and John Bergman for helpful discussions. Computer time was provided by the NOAA Forecast Systems Laboratory High Performance Computing Center. This work was supported in part by a grant from NOAA's Office of Global Programs.

APPENDIX

Energy Budget Notation

The column-integrated energy budget for an atmospheric column (with no ocean energy transport) may be written as follows (e.g., see Sun et al. 2003):

$$S - F + D = S^{\text{clear}} - \sigma T^4 + G_w + C_L + C_S + D = N_{\text{O}}, \quad (1)$$

where S is net insolation (TOA), F is outgoing longwave radiation (TOA), T is surface temperature, σ is Stefan–Boltzmann constant, D is dynamical energy convergence in the atmosphere, and N_{O} is net heat flux into the ocean. Superscript clear denotes clear-sky values, otherwise total values are assumed. We also adopt the standard definitions of shortwave cloud forcing, $C_S = S - S^{\text{clear}}$, longwave cloud forcing: $C_L = -(F - F^{\text{clear}})$, and clear-sky greenhouse effect: $G_W = \sigma T^4 - F^{\text{clear}}$. For global quantities, as shown in section 5 of this paper, the dynamical term integrates to zero.

In the absence of ocean dynamics, the surface energy budget decouples from the atmospheric energy budget. We may decompose the surface energy budget in a manner similar to that of the atmospheric column as follows:

$$N_{\text{O}} = S_{\text{O}}^{\text{clear}} - \sigma T^4 + G_{\text{WO}} + C_{\text{LO}} + C_{\text{SO}} - F_{\text{TO}}, \quad (2)$$

where subscript O denotes (ocean) surface values, and F_{TO} is the net (upward) turbulent flux of latent and sensible heat from ocean to atmosphere. As above, we have $C_{\text{SO}} = S_{\text{O}} - S_{\text{O}}^{\text{clear}}$, $C_{\text{LO}} = -(F_{\text{O}} - F_{\text{O}}^{\text{clear}})$, and $G_{\text{WO}} = \sigma T^4 - F_{\text{O}}^{\text{clear}}$. We may combine Eqs. (1) and (2) to yield

$$-D = (C_S - C_{\text{SO}}) + (S^{\text{clear}} - S_{\text{O}}^{\text{clear}}) + (G_W - G_{\text{WO}}) + (C_L - C_{\text{LO}}) + F_{\text{TO}}.$$

In other words, the atmospheric dynamics is in balance with the heat "trapped" by the greenhouse effect of water vapor and clouds, less the amount sent back to the surface, plus the turbulent fluxes. Note that connections between the dynamics and *individual* components of the surface energy budget are not constrained by the energy budget.

REFERENCES

Chýlek, P., and J. T. Kiehl, 1981: Sensitivities of radiative–convective models. *J. Atmos. Sci.,* **38,** 1105–1110.

Covey, C., K. M. ArchutaRao, U. Cubasch, P. Jones, S. J. Lambert, M. E. Mann, T. J. Phillips, and K. E. Taylor, 2003: An Overview of results from the coupled model intercomparison project (CMIP). *Global Planet. Change,* **37,** 103–133.

Held, I. M., and B. J. Soden, 2000: Water vapor feedback and global warming. *Ann. Rev. Energy Environ.,* **25,** 441–475.

Hess, P. G., D. S. Battisti, and P. J. Rasch, 1993: Maintenance of the intertropical convergence zones and the large-scale tropical circulation on a water covered Earth. *J. Atmos. Sci.,* **50,** 691–713.

Kirtman, B. P., and E. K. Schneider, 2000: A spontaneously generated tropical atmospheric general circulation. *J. Atmos. Sci.,* **57,** 2080–2093.

Langen, P. L., and V. A. Alexeev, 2004: Multiple equilibria and asymmetric climates in the CCM3 coupled to an oceanic mixed layer with thermodynamic sea ice. *Geophys. Res. Lett.,* **31,** L04201, doi:10.1029/2003GL019039.

Larson, K., and D. L. Hartmann, 2003a: Interactions among cloud, water vapor, radiation and large-scale circulation in the tropical climate. Part I: Sensitivity to uniform sea surface temperature changes. *J. Climate,* **16,** 1425–1440.

——, and ——, 2003b: Interactions among cloud, water vapor, radiation and large-scale circulation in the tropical climate. Part II: Sensitivity to spatial gradients of sea surface temperature. *J. Climate,* **16,** 1441–1455.

Li, T., 1997: Air–sea interactions of relevance to the ITCZ: Analysis of coupled instabilities and experiments in a hybrid coupled GCM. *J. Atmos. Sci.,* **54,** 134–147.

Lindzen, R. S., and A. Y. Hou, 1988: Hadley circulations for zonally averaged heating centered off the Equator. *J. Atmos. Sci.,* **45,** 2416–2427.

——, ——, and B. F. Farrell, 1982: The role of convective model choice in calculating the climate impact of doubling CO_2. *J. Atmos. Sci.,* **39,** 1189–1205.

Manabe, S., and R. T. Wetherald, 1967: Thermal equilibrium of the atmosphere with a given distribution of relative humidity. *J. Atmos. Sci.,* **24,** 241–259.

Neale, R. B., and B. J. Hoskins, 2000: A standard test for AGCMs including their physical parametrizations. Part I: The proposal. *Atmos. Sci. Lett.,* **1,** 101–107.

Raymond, D. J., 2000: The Hadley Circulation as a radiative–convective instability. *J. Atmos. Sci.,* **57,** 1286–1297.

Sun, D.-Z., J. Fasullo, T. Zhang, and A. Roubicek, 2003: On the radiative and dynamical feedbacks over the Equatorial Pacific Cold Tongue. *J. Climate,* **16,** 2425–2432.

Waliser, D. E., and R. C. J. Somerville, 1994: Preferred latitudes of the Intertropical Convergence Zone. *J. Atmos. Sci.,* **51,** 1619–1639.

Xie, S.-P., and S. G. H. Philander, 1994: A coupled ocean–atmosphere model of relevance to the ITCZ in the eastern Pacific. *Tellus,* **46A,** 340–350.